Heat/Mass Transfer Characteristics in Angled Ribbed Channels With Various Bleed Ratios and Rotation Numbers

Kyung Min Kim
Suk Hwan Park
Yun Heung Jeon
Dong Hyun Lee
Hyung Hee Cho
e-mail: hhcho@yonsei.ac.kr

Department of Mechanical Engineering,
Yonsei University,
Seoul 120-749, Korea

The present study investigates the effects of secondary flow due to angled rib turbulators on the heat/mass transfer in the square channels with channel rotation and bleed flow. The angle of attack of the angled ribs was 45 deg. The bleed holes were located between the rib turbulators on either the leading or trailing surface. The tests were conducted under the conditions corresponding to various bleed ratios (BR = 0.0, 0.2, and 0.4) and rotation numbers (Ro = 0.0, 0.2, and 0.4) at Re = 10,000. The results suggest that the heat/mass transfer characteristics were influenced by the Coriolis force, the decrement of the main flow rate, and the secondary flow. In the 90 deg angled ribbed channel, the heat/mass transfer reduced on the leading surface with an increment in the rotation number, but it increased on the trailing surface. However, it decreased on both surfaces in the 45 deg angled ribbed channel. As the bleed ratio increased, the Sherwood number ratios decreased on both the bleeding and nonbleeding surfaces for the 45 deg angled ribs but increased on the bleeding surface for the 90 deg angled ribs.
[DOI: 10.1115/1.2777196]

Introduction

In the development of high performance gas turbine engines, designing an effective cooling system is crucial. Therefore, the turbine inlet temperature has been increased steadily to improve the thermal efficiency of the turbine engines: however, this resulted in high heat loads on the turbine blades. To protect the blade materials from damage due to heating beyond the maximum allowable temperature, various cooling techniques have been employed. Among these techniques, internal passage cooling is used for cooling the inner turbulated surface; this was achieved using cooling air generated by a compressor. Film cooling is performed to protect the blade surfaces in contact with hot gases by using cooling air ejected through the holes on the blade surface after cooling internal passages. The bleed flow, flow structures, and heat transfer generated by the cooling air in the internal passage show differences. Moreover, when the turbine blades rotate, the Coriolis force causes greater variations in the flow structures; hence, it becomes necessary to understand how those parameters affect the cooling performance.

To promote heat transfer and cooling performance in the internal cooling passages, various cooling techniques (rib turbulator, pin fin, dimple, etc.) have been studied. Among these techniques, the technique of using repeated rib turbulators has been actively investigated since the early 1970s. Moreover, after Han et al. [1] reported that the repeated 45 deg angled ribs performed better than repeated 90 deg angled rib in a parallel-plate channel, many researchers [2–6] have studied the effects of various rib conditions such as rib height, rib angle of attack, rib-to-rib pitch, rib shape, and rib arrangement on the heat transfer and the flow structures using many measurement techniques.

In a practical cooling passage with rotor blades, the heat transfer distributions are significantly affected by rotational forces (Coriolis and rotating buoyancy forces), which produce secondary flow and force heavier cooling fluid to flow away from the center of rotation. The rotational effects on heat transfer have been experimentally reported by many researchers [7–10]. They explained that these force deflect the coolant fluid toward the trailing surface, in the case of outward flow, and toward the leading surface, in the case of inward flow. Thus, heat transfer discrepancy between the leading and trailing surfaces results.

In most modern turbine blades, the cooling passages have rib turbulators for heat transfer enhancement and ejection holes for film cooling. Bleed holes are formed on the blade surface and they have significant effects on the heat transfer in the cooling passage. Therefore, studying the effects of bleed flow is essential. Many researchers [11–14] measured the local heat transfer coefficients in stationary channels with bleed holes, and reported that the bleed flow on the surface yields higher heat transfer around the holes; further, they have lower friction factor than that under no bleed condition. They also reported that placing the bleed holes after the ribs widened the regions of high heat transfer because the recirculation flow behind the ribs was eliminated.

However, most of the studies on the heat transfer characteristics in the internal passages with bleed holes were conduced under stationary conditions. Therefore, to understand the cooling system of them, it is necessary to study the heat transfer characteristics under rotating conditions. Regarding this, Kim et al. [15] and Jeon et al. [16] have studied the effects of bleed flow on the detailed heat/mass transfer distributions in smooth and 90 deg angled ribbed channels under various rotating conditions. In the present study, to experimentally obtain the effects of an additional secondary flow, we measured the local heat/mass transfer distributions in rotating channels with 45 deg angled rib turbulators and various bleed flows; we then compared them with the data of the 90 deg angled ribbed cases.

Contributed by the International Gas Turbine Institute of ASME for publication in the JOURNAL OF TURBOMACHINERY. Manuscript received June 7, 2007; final manuscript received June 19, 2007; published online May 6, 2008. Review conducted by David Wisler. Paper presented at the ASME Turbo Expo 2007: Land, Sea and Air (GT2007), 2007, Montreal, Quebec, Canada, May 14–17, 2007, Paper No. GT2007-27166.

Experimental Apparatus

Rotating Facility. A schematic view of the experimental apparatus is shown in Fig. 1. The test rig was comprised of a blowing system, a rotating system, and a measuring system. First, in the

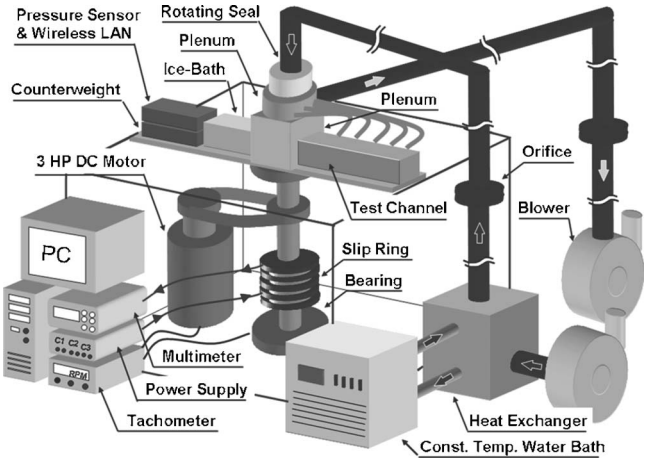

Fig. 1 Experimental apparatus

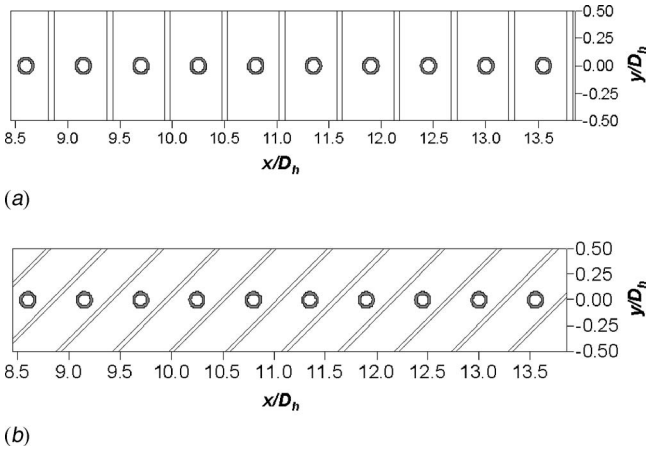

Fig. 3 Coordinate system of the test section with bleed holes: (*a*) 90 deg angled ribbed channel and (*b*) 45 deg angled ribbed channel

case of the blowing system, one blower supplied room air into the test section and another blower supplied the bleed flow through the test section. These blowers were controlled using frequency inverters. Air temperature was regulated during the experiment using a heat exchanger. The blowing and bleeding flows were measured by orifice flow meters. The Reynolds number (Re), which is based on the hydraulic diameter and the ratio of the bleed flow to the main flow (bleed ratio, BR), was monitored, and it was observed to be constant during the tests. The maximum difference in the bleed flow through each bleed hole was verified to be within 3% for all the cases by differential pressure tests. A magnetic rotating seal and a rib seal were equipped in order to prevent any leakage through the rotating parts. A 3 hp (2.24 kW) dc motor connected with to a V-belt drove the rotating shaft, whose rotation speed was measured by an optical tachometer. Rotation numbers remained 0.0, 0.2, and 0.4 during the tests. The maximum rotation number (Ro=0.4) corresponded to 400 rpm approximately. Lastly, for a measuring system (an Agilent data logger and a low pressure differential sensor by GE Druck) interfaced to a computer via slip rings and wireless LAN equipment, electrical output signals were recorded from the test sections. For accurate measurements of the naphthalene surface temperature, J-type thermocouples were embedded in the test plate because the vapor pressure of naphthalene is sensitive to temperature, and varies by about 10% change per °C. The temperature of the bulk air was also obtained by the thermocouples installed in the channel inlets and outlets.

Test Section. Figure 2 shows the geometry of the test channel

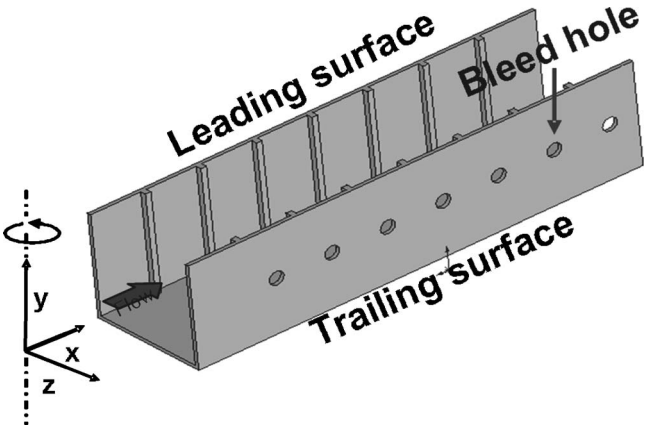

Fig. 2 Geometry of the test channel with 90 deg angled ribs

with 90 deg rib turbulators and Fig. 3 shows the coordinate system of the test section. As shown in Table 1, the test channel had a hydraulic diameter (D_h) of 40.0. Further, its streamwise coordinate ranges from $x/D_h=8.45$ to $x/D_h=13.8$. The square rib turbulators were installed on both leading and trailing surfaces of the test channel and their array were inlined. The rib height-to-hydraulic diameter ratio (e/D_h) was 0.055 and the rib-to-rib pitch (p/e) was 10.0 times that of the rib height. Each bleed hole was located at the center of the rib turbulators on either leading or trailing surfaces; there were 20 holes each having a diameter (d) of 4.5 mm. The ratio of the hole spacing to the diameter (p_h/d) was 4.9. The ratio of the maximum rotating radius to the hydraulic diameter (R/D_h) was 14.5. The coordinate systems of the test sections are shown in Figs. 3(a) and 3(b). The streamwise, lateral, and vertical directions corresponded to the x, y, and z axes, respectively. The test section was covered with naphthalene from $x/D_h=8.45$ to $x/D_h=13.8$ and had ten bleed holes. The lateral domain ranged from $y/D_h=-0.5$ to $y/D_h=0.5$.

To measure the pressure drop across the channel, pressure tests were conducted by using an electronic pressure sensor. Eight pressure taps were drilled at $z/D_h=0.0$ on one of the sidewalls, with a spacing and a diameter of 66 mm and 0.8 mm, respectively.

Procedure and Data Reduction

A naphthalene sublimation method was employed to obtain detailed heat/mass transfer coefficients using the analogy between heat and mass transfer. The surfaces of the test section were cast with naphthalene to simulate heating condition of a cooling passage in a gas turbine blade. Naphthalene surfaces where mass transfer occurred correspond to a uniform wall temperature

Table 1 Test section configurations

Hydraulic diameter (D_h)	40.0 mm
Passage height (H)	40.0 mm
Passage width (W)	40.0 mm
Max. rotating radius (R)	580 mm
Test section length	552 mm
Naph. coated length	214 mm
Bleed hole diameter (d)	4.5 mm
Rim thickness of hole	1.0 mm
Hole-to-hole pitch (p_h)	22.0 mm
Rib height (e)	2.2 mm
Rib-to-rib pitch (p)	22.0 mm
Attack angle of rib (α)	45 deg or 90 deg

boundary condition of heat transfer experiments. The local naphthalene sublimation depth was measured to attain mass transfer coefficients on each position using a liner variable differential transformer LBB-375TA-020 and an automated positioning table. It is expressed as

$$h_m = \frac{\dot{m}}{\rho_{v,w} - \rho_{v,b}} = \frac{\rho_s(\Delta z/\Delta t)}{\rho_{v,w} - \rho_{v,b}} \tag{1}$$

where $\dot{m}$ is the local mass transfer rate of naphthalene per unit area, and $\rho_{v,w}$ and $\rho_{v,b}$ are the vapor density at the naphthalene surface and the bulk vapor density of naphthalene, respectively. From the local mass transfer coefficient, the Sherwood number is calculated as

$$\mathrm{Sh} = h_m D_h / D_{\mathrm{naph}} \tag{2}$$

where D_{naph} is the diffusion coefficient of naphthalene in air. The properties of naphthalene suggested by Ambrose et al. [17] and Goldstein and Cho [18] are used in the present study. The uncertainty in the Sherwood number is estimated to be within $\pm 8.0\%$ at a 95% confidence level using the uncertainty estimation method of Kline and McClintock [19]. The Nusselt numbers can be obtained from the Sherwood numbers by the correlation $\mathrm{Nu}/\mathrm{Sh} = (\mathrm{Pr}/\mathrm{Sc})^{0.4}$, which is for turbulent flows.

The mass transfer results are presented as the Sherwood number ratios $\mathrm{Sh}/\mathrm{Sh}_0$ to estimate the heat/mass transfer augmentation effectively, where Sh_0 is the Sherwood number for a fully developed turbulent flow in a stationary smooth circular tube correlated by McAdams [20] and converted to mass transfer parameters as

$$\mathrm{Sh}_0 = 0.023\mathrm{Re}^{0.8}\mathrm{Sc}^{0.4} \tag{3}$$

The averaged Sherwood numbers, such as $\overline{\mathrm{Sh}}_p$, $\overline{\mathrm{Sh}}_R$, and $\bar{\bar{\mathrm{Sh}}}_R$ are calculated by the integration of the local Sherwood numbers weighted by constant area (between rib turbulators and from $x/D_h = 10.5$ to 13.25).

The average pressure drop is obtained from the slope calculated by a linear curve fitting of the local pressure difference data in the middle region of the channel ($\Delta P/\Delta L$) where the static pressure decreases linearly. The friction factor is calculated with the average pressure drop as

$$f = \Delta P / [4(\Delta L/D_h)(1/2)\rho u_b^2] \tag{4}$$

The uncertainty of the friction factor is within 4.4%. The friction loss results are presented as the friction factor ratios f/f_0, where f_0 represents the friction factor for a fully developed turbulent flow in a stationary smooth circular tube. The empirical equation that closely fits the Kármán–Nikuradse equation proposed by Petukhov [21] is employed as $f_0 = 2(2.236 \ln \mathrm{Re} - 4.639)^{-2}$.

The thermal performance η obtained by considering both the heat/mass transfer augmentation and the friction loss increment is presented based on the constant pumping power condition and it is expressed as the following equation:

$$\eta = (\bar{\bar{\mathrm{Sh}}}_R/\mathrm{Sh}_0)/(f/f_0)^{1/3} \tag{5}$$

The detailed experimental procedure and data reduction are described in Kim et al. [15] and Jeon et al. [16].

Results and Discussion

Heat/Mass Transfer Characteristics

Cases With 90 deg Angled Rib Turbulators. Figure 4 shows the local Sherwood number ratio distributions in the channel with transverse ribs and bleed flow. The contours in this figure are presented in the range of $11.5 \leq x/D_h \leq 13.0$ due to the periodic patterns in the fully developed region.

When the rotation number was 0.0 (Fig. 4(*a*); stationary case), the high heat/mass transfer coefficients appeared in an inter-rib region on the nonbleeding surface due to the transverse ribs. The peak appeared at the upstream of the middle of the inter-rib region

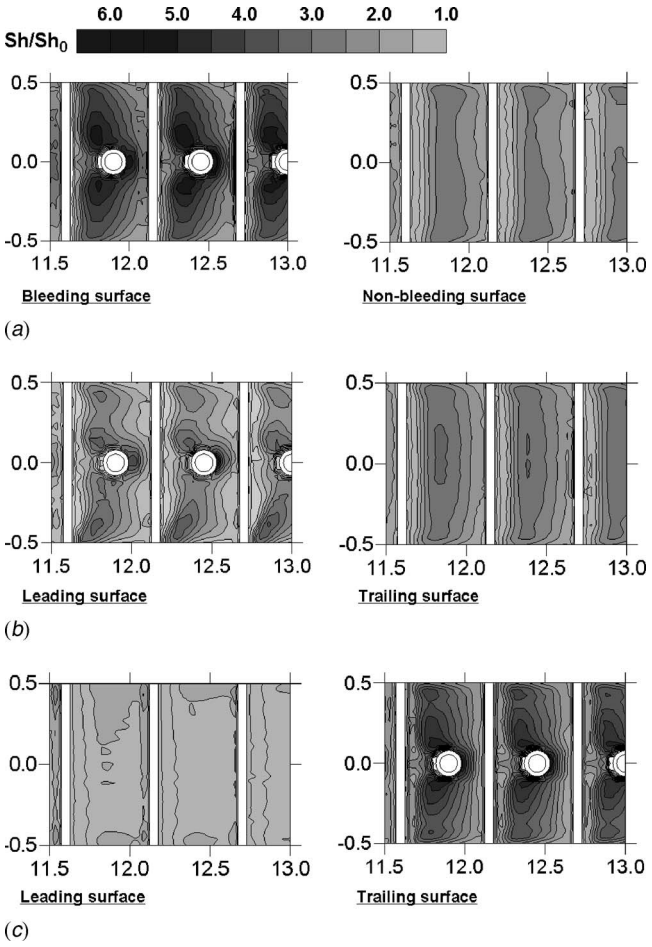

Fig. 4 The local $\mathrm{Sh}/\mathrm{Sh}_0$ distributions in the 90 deg angled ribbed channel with bleed flow (BR=0.4): (*a*) Ro=0.0, (*b*) Ro=0.4 (bleeding on the leading surface), and (*c*) Ro=0.4 (bleeding on the trailing surface)

due to the reattachment of the flows passing over the ribs. The lateral distributions were uniform except the corner of the passage. In these corner regions, the heat/mass transfer decreased due to weakened reattachment as a result of the redevelopment of flows caused by the wall friction. This is a typical pattern of the heat/mass transfer distributions on ribbed surfaces with flow separation and reattachment, and this pattern agreed well with the results of the previous studies such as Kukreja et al. [2], Aliaga et al. [3], and Acharya et al. [4]. On the bleeding surface with bleed holes, the heat/mass transfer was higher than that on the nonbleeding surface because the reattachment became strong around the holes due to the effect of the tripping flow, which impinges around the bleed holes due to the drawing flow by suction and augments the heat/mass transfer on the vicinity of them.

When the passage rotates (Figs. 4(*b*) and 4(*c*); Ro=0.4), in general, the heat/mass transfer decreases on the leading surface but increases on the trailing surface [7–11]. In other words, for the leading surface on the middle region except for the corners of the passage and the regions around the holes, the reattachment became weak due to the Coriolis force acting on the trailing surface. On the corner regions, a high heat/mass transfer appeared due to the impingement of the secondary flow returning from the trailing surface due to the Coriolis force. In the overall trailing surface region, the heat/mass transfer increased because the separated flow by the rib turbulators was reattached strongly by the Coriolis force

For cases with bleed flow on the leading surface (Fig. 4(*b*)), the heat/mass transfer decreased in the middle region of the leading

surface due to the Coriolis force acting on the trailing surface. The Sherwood number ratios around the holes were high due to the tripping flow, although the values were lower than those at Ro =0.0. For the entire trailing surface region, the heat/mass transfer without rotation and bleed flow was augmented by the Coriolis force. When bleed flow occurred on the trailing surface (Fig. 4(*c*)), the heat/mass transfer patterns were similar to those of Ro =0.0 for both the bleeding and nonbleeding surfaces. The heat/mass transfer on the nonbleeding (or leading) surface had a lower value. However, on the bleeding (or trailing) surface, the Sherwood number ratios were locally augmented in the corner region and almost identical to those in the middle region.

The pitch-averaged Sherwood number ratios obtained from the local experimental data among all the rib turbulators except those on the rib surface are shown in Fig. 5. The figure presents the averaged heat/mass transfer along the streamwise direction in the whole measured region at each rotation and bleed ratio.

In the stationary case (Fig. 5(*a*)), the fully developed values at BR=0.0 were enhanced greater than in the fully developed values (Sh_0) for a stationary smooth circular tube by approximately 2.7. In the case of BR=0.2, the heat/mass transfer on the leading (or bleeding) surface was increased by the effect of the tripping flow that occurs around the bleed holes due to the suction drawing flow, in contrast, the effect on the trailing (or nonbleeding) surface decreased by the reduction of the main flow. Further, the averaged values on both the surfaces decreased as the flow proceeded because of the continuous bleeding. As the bleed ratio increased, the heat/mass transfer coefficients on the leading surface gradually increased but those on the trailing surface decreased.

In the case of rotation with bleeding on the leading surface (Fig. 5(*b*)), the Coriolis force augmented the heat/mass transfer on the trailing surface onto which the coolant flow was deflected but deteriorated that on the leading surface. However, as the bleed ratio increased, the discrepancy between the heat/mass transfer coefficients of the leading and the trailing surfaces decreased due to the tripping flow effect. This was because the heat/mass transfer is enhanced on the bleeding surface but was reduced on the nonbleeding surface. In the case of rotation with bleeding on the trailing surface (Fig. 5(*c*)), the difference in heat transfer between the surfaces increased to more than that for BR=0.0 with an increment in the bleed ratio. In particular, the averaged coefficients on the nonbleeding (or leading) surface considerably reduced due to the reduction of the main flow and the deflection toward the trailing surface. However, the heat/mass transfer on the bleeding (or trailing) surface was almost identical because the main secondary flow moved toward the trailing surface.

Figure 6 shows the regional averaged Sherwood number ratios obtained from the local data between $x/D_h=10.5$ and 13.25 except for those on the rib surface. The averaged values taken from the fully developed five pitch regions at each rotation number and bleed ratio. The present data are compared to averaged heat transfer data obtained by Ekkad et al. [14,22] on the bleed surface in the first pass of the stationary channel with 90 deg ribs. Although the averaged values of the present study were higher than data by Ekkad et al. [14,22] due to different experimental conditions as introduced in Table 2, the values by bleed flow were enhanced. In the case of bleeding on the leading surface (Fig. 6(*a*)), as the rotation numbers increased, the heat/mass transfer on the leading surface gradually decreased; however, that on the trailing surface increased gradually. In the case of the bleed flow, for any rotation numbers, the values on the leading (or bleeding) surface were enhanced by the tripping flow. However, those on the trailing (or nonbleeding) surface were reduced by the reduction of the main flow. For bleeding on the trailing surface (Fig. 6(*b*)), as the rotation number and bleed ratios increased, the heat/mass transfer on the leading surface decreased whereas that on the trailing surface increased. In other words, the channel rotation and tripping flow caused a large difference in the average values between the leading and trailing surfaces.

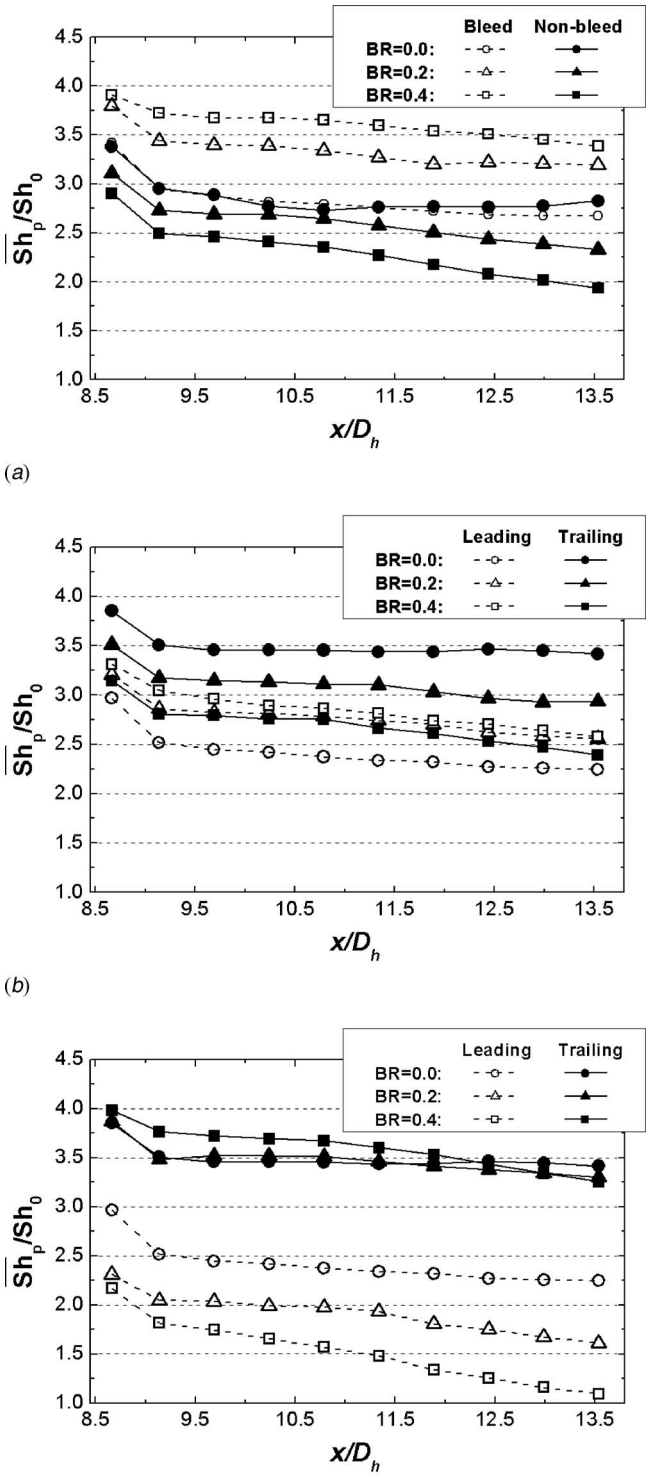

Fig. 5 Pitch averaged Sh/Sh_0 distributions in the 90 deg angled ribbed channel: (*a*) Ro=0.0, (*b*) Ro=0.4 (bleeding on the leading surface), and (*c*) Ro=0.4 (bleeding on the trailing surface)

Cases With 45 deg Angled Rib Turbulators. In this section, to investigate the secondary flow induced by angled rib turbulators, the experimental data for the 90 deg angled ribbed channels were used for comparison. Figure 7 shows the local Sherwood number ratio distributions in the channels with the 45 deg angled ribs and

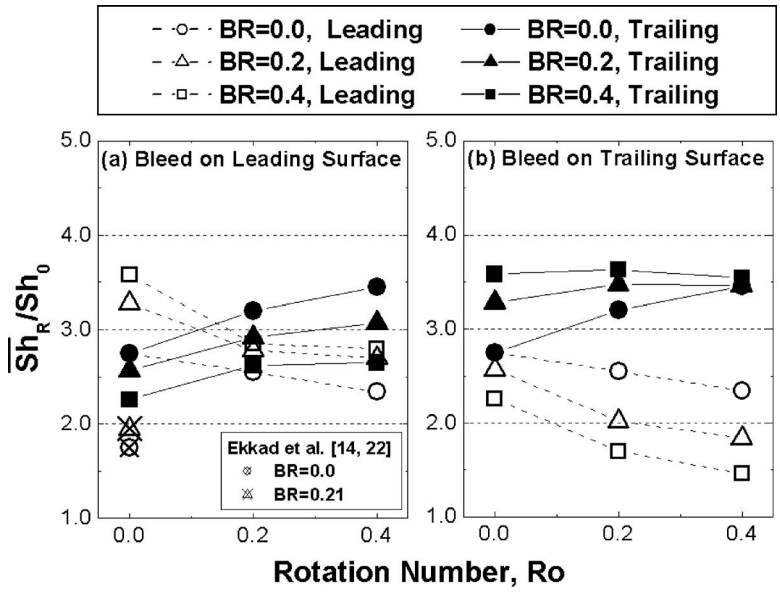

Fig. 6 Regional averaged Sh/Sh_0 ($10.5 \leq x/D_h \leq 13.25$) for all the tests in the 90 deg ribbed channel

bleed flow. The contours in this figure are presented in the range of $11.5 \leq x/D_h \leq 13.0$ due to the periodic patterns in the fully developed region.

In the stationary case (Fig. 7(*a*); Ro=0.0), high Sherwood number ratios were observed in the downward region ($-0.5 \leq y/D_h \leq -0.2$) of the secondary flow induced by the angled rib turbulators. These secondary flows moved along the angled ribs near the ribbed walls and then moved upwards near the one of the sidewall at $y/D_h=0.5$. In the results, downward flows were induced near the opposite side wall, $y/D_h=-0.5$. The secondary flows were induced near the opposite ribbed wall as well, which resulted in the creation of counter-rotating secondary flow cell pairs. Further, the high heat/mass transfer regions around the holes in the bleeding (or leading) surface appeared to be larger than those on the nonbleeding (or trailing) surface because the secondary flows strongly reattached due to the effect of the tripping flow.

Although the passage was rotated, the heat/mass transfer patterns were similar to those in the stationary case. This is because an additional vortex was not generated by the Coriolis force. In other words, a pair of vortices in the 90 deg ribbed channels was generated. In the 45 deg ribbed channels, although the channel rotation deflected the flow by acting on the one surface, the vortex flow was not caused. Thus, the low heat transfer regions appear on the entire opposite surface region. For cases with the bleed flow on the leading surface (Fig. 7(*b*)), the heat/mass transfer decreased in the middle region of the leading surface, but was large around the holes. On the trailing surface, the heat/mass transfer was augmented by the rotation, and the low heat transfer regions ranged

Table 2 Experimental conditions for data validation

	Present study	Ekkad et al. [14,22]
Experiment	Mass transfer	Heat transfer
D_h	40.0 mm	50.8 mm
W/H	1.0	1.0
e/D_h	0.055	0.125
p/e	10.0	10.0
α	45 deg, 90 deg	60 deg, 90 deg
d	4.5 mm	6.3 mm
Re	10,000	12,000
BR	0.0, 0.2, 0.4	0.0, 0.21

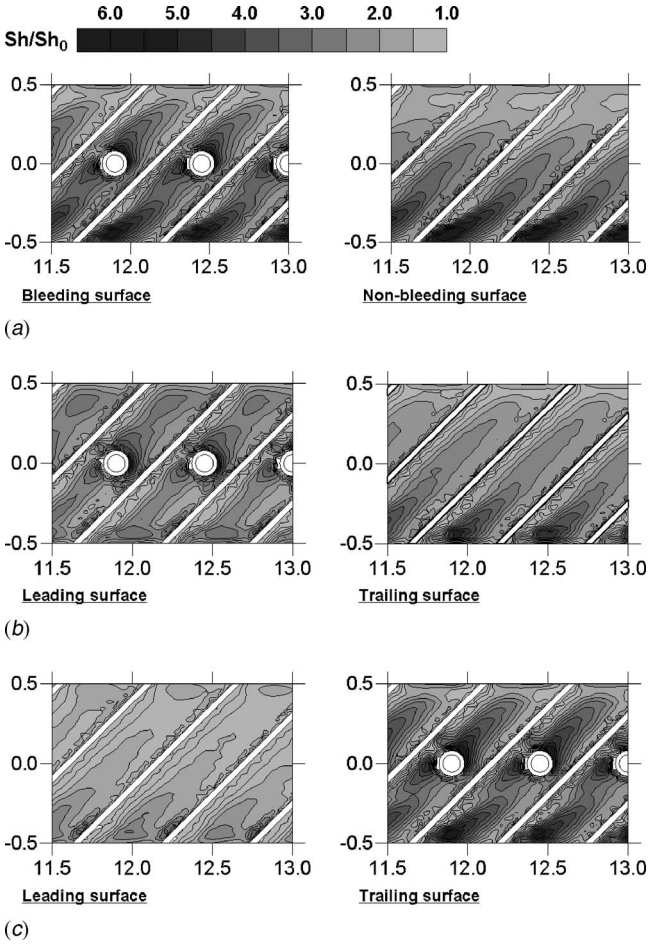

Fig. 7 The local Sh/Sh_0 distributions in the 45 deg angled ribbed channel with bleed flow (BR=0.4): (*a*) Ro=0.0, (*b*) Ro =0.4 (bleeding on the leading surface), and (*c*) Ro=0.4 (bleeding on the trailing surface)

from $y/D_h=0.0$ to 0.5, as shown in Fig. 7(*a*); further, these became narrower, as shown in Fig. 7(*b*). However, because of the decrement in the main flow rate, the Sherwood number ratios were lower than those of Ro=0.0. In the case of bleeding on the trailing surface (Fig. 7(*c*)), due to the bleed flow and Coriolis force, although the low heat/mass transfer regions appeared on the leading surface, the high regions were observed on the trailing surface.

Figure 8 shows the pitch-averaged Sherwood number ratios obtained from the local experimental data among the rib turbulators except for those on the rib surface. The figure presents the averaged heat/mass transfer along the streamwise direction in the whole measured region at each rotation and bleed ratio.

In a stationary channel with the 45 deg angled ribs (Fig. 8(*a*)), the fully developed values of BR=0.0 were higher than the fully developed values in the 90 deg angled ribbed channel (Fig. 5(*a*)) by approximately 18%. In cases with the bleed flow (BR=0.2 and 0.4), the heat/mass transfer in the upstream part ($8.5 \leqslant x/D_h \leqslant 9.5$) of the leading (or bleeding) surface was similar to the case of BR=0.0. In the downstream part ($11.5 \leqslant x/D_h \leqslant 13.5$) of the leading surface, the values were lower than those at BR=0.0. This was because the main flow rate reduced regularly as the flow continued. However, the values on the leading surface were not enhanced by the tripping flow in contrast to the 90 deg angled ribbed cases because of the angled rib-induced secondary flow. However, on the trailing surface, due to the reduction of the main flow, the Sherwood number ratios decreased gradually as the bleed ratios increased.

In the rotating channel with nonbleeding and 45 deg angled ribbed surfaces, the disparity of the heat/mass transfer between the leading and trailing surfaces was smaller than that in the 90 deg angled ribbed rotating channels. In other words, the increase in the rate of the heat/mass transfer on the trailing surface was less than that in the 90 deg angled ribbed cases. This is because the secondary flow induced by the angled rib turbulators was strong. In the case of bleeding on the leading surface (Fig. 8(*b*)), the heat/mass transfer was augmented in the upstream part ($8.5 \leqslant x/D_h \leqslant 9.5$) of the leading surface, but reduced in the downstream part ($11.5 \leqslant x/D_h \leqslant 13.5$) of the leading surface. Similar to the 90 deg angled ribbed channels, as the bleed ratios increased, the heat/mass transfer coefficients on the trailing surfaces were decreased by the reduction of the main flow. In the case of bleeding on the trailing surface (Fig. 8(*c*)), with an increment in the bleed ratio, the heat/mass transfer difference between the leading and trailing surfaces was more increased than that of BR=0.0. This phenomenon was similar to that in the 90 deg ribbed cases.

Figure 9 shows the regional averaged Sherwood number ratios obtained from the local data between $x/D_h=10.5$ and 13.25 except for those on the rib surface. The averaged values taken from the fully developed five pitch regions at each rotation number and bleed ratio. The present data are also compared to averaged heat transfer data obtained by Ekkad et al. [14,22] on the bleed surface in the first pass of the stationary channel with 45 deg ribs. Unlike the 90 deg ribbed case, the averaged values of the present study were higher than data by Ekkad et al. [14,22] and were reduced by bleed flow. For all the tests with angled ribs, with an increment in the rotation number, the decreasing rate of the heat/mass transfer on the leading and trailing surfaces was identical. As the bleed ratio increased, the averaged Sherwood number ratios reduced at a fixed rate. This was because the heat/mass transfer on the ribbed walls is significantly affected by the Coriolis force and main flow rate.

Figure 10 shows the mean Sherwood number ratios of both the leading and trailing surfaces at tested rotation number and bleed ratios. In the stationary cases, the mean values of the 45 deg angled ribbed cases were higher than those of the 90 deg angled ribbed cases because of the strong secondary flow induced by the angled ribs. Except for the 90 deg angled ribbed cases without the bleed flow, as the rotation number increased, the values decreased because of the Coriolis force that disturbed the reattachment of the main flow and the bleeding that reduced the flow rate. For the 90 deg angled ribbed cases without bleed flow, the values increased since the rotation-induced secondary flow enhanced the heat/mass transfer. In particular, in the channel with the 45 deg

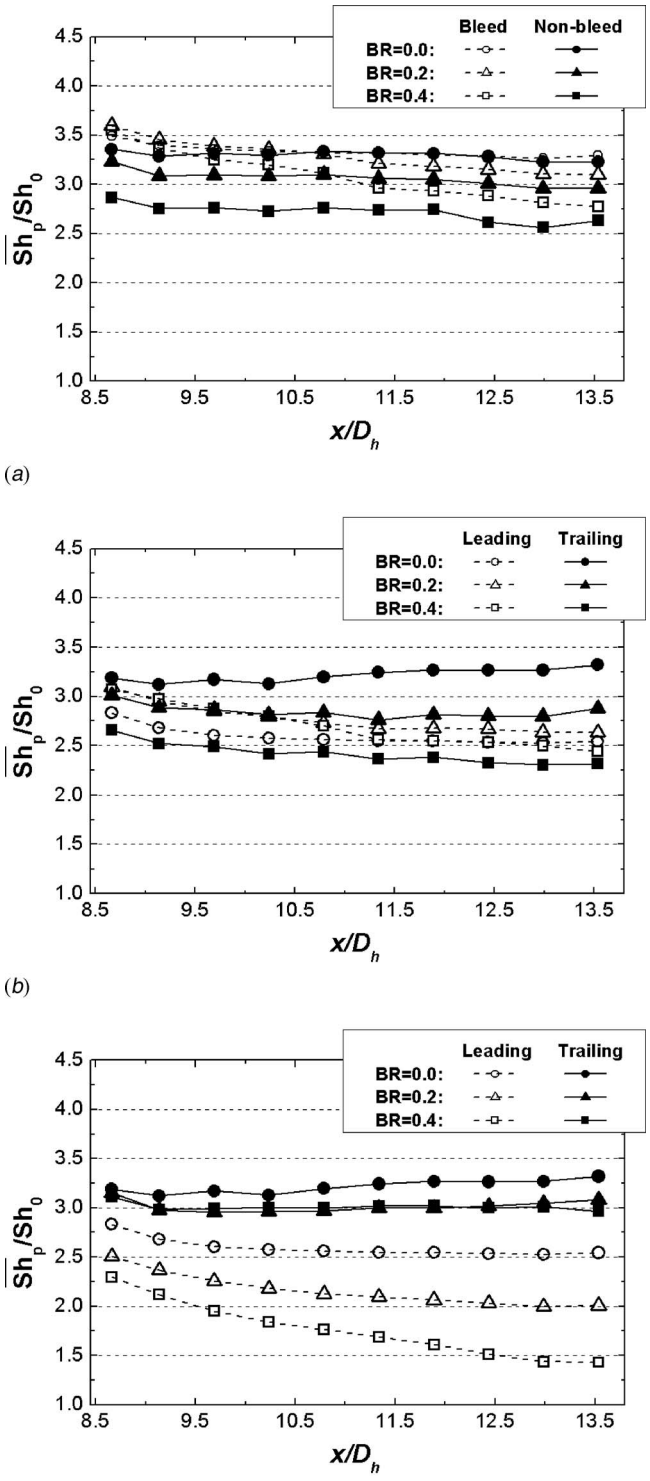

Fig. 8 Pitch averaged Sh/Sh_0 distributions in the 45 deg angled ribbed channel: (*a*) Ro=0.0, (*b*) Ro=0.4 (bleeding on the leading surface), and (*c*) Ro=0.4 (bleeding on the trailing surface)

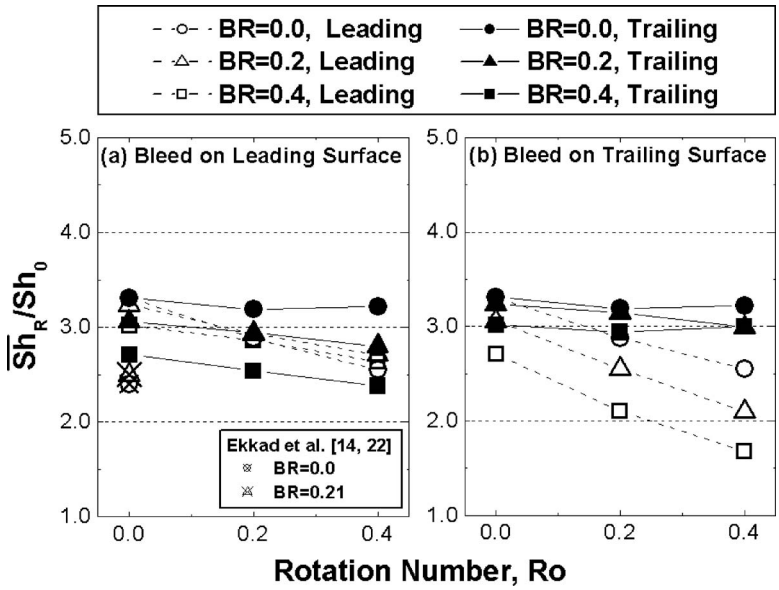

Fig. 9 Regional averaged Sh/Sh_0 ($10.5 \leq x/D_h \leq 13.25$) for all the tests in the 45 deg ribbed channel

angled rib turbulators, for the bleeding on the trailing surface, the higher rotation number or higher bleed ratios decreased the mean values.

Friction Loss and Performance. Figure 11 shows the friction loss results in the form of the friction factor ratios. As the rotation number increased, the friction factors gradually increased in only the 90 deg angled ribbed cases without bleed flow, but decreased in the other cases. This is because the turbulence intensity is strengthened to a greater extent by the rotation-induced secondary flow in cases with transverse ribs and nonbleeding surfaces. However, in cases with bleeding flow and angled ribs, the main flow rate was reduced and the angled rib-induced secondary flow was disturbed by deflection of the core flow. In the case of the bleed flow, the friction factor ratios decreased in all the tested cases. The declination resulted from the reduction of the internal flow due to the bleed flow and reduction in the area (of the bleed holes) where the flow contacted.

Figure 12 shows the thermal performance in the two ribbed channels. The thermal performance with both angled ribs and bleed flow was the highest for all the rotation numbers. This is because the heat/mass transfer was significantly enhanced by the angled rib turbulators and the friction factor decreased with the bleed flow. As the rotation number increased, the thermal performance for all the cases was almost identical even though the heat/mass transfers and the pressure drops were different for each channel.

Conclusions

In the present study, the heat/mass transfer characteristics in rotating angled ribbed channels with the bleed flow were experimentally investigated and compared with the 90 deg angled ribbed cases. The results are summarized as follows.

1. For cases without the bleed flow, the Sherwood number ratios were enhanced by approximately 2.7 and 3.3 times more than Sh_0 due to the transverse and angled ribs, respectively.

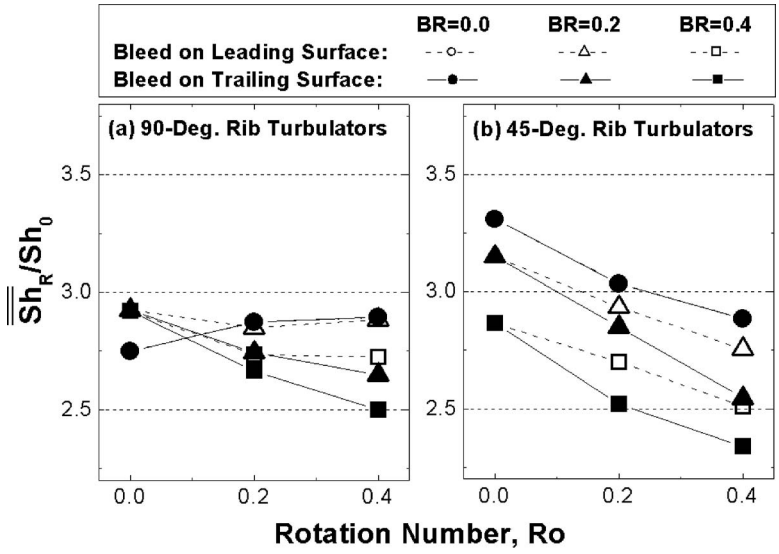

Fig. 10 Mean Sh/Sh_0 of the leading and trailing surfaces

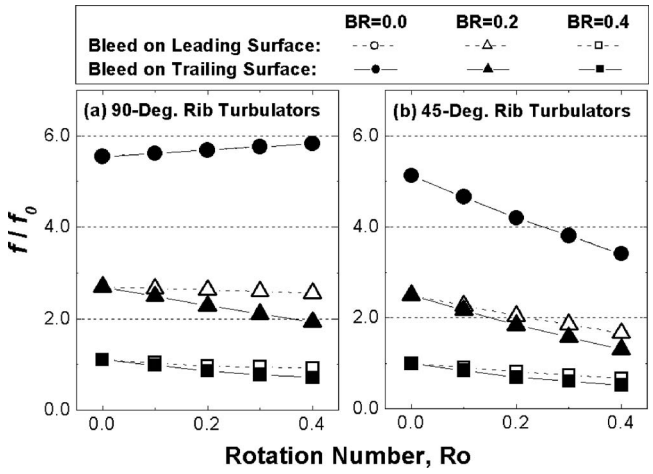

Fig. 11 Friction factor ratios at various rotation numbers

The heat/mass transfer in the 90 deg angled ribbed cases was augmented by the rotation-induced secondary flow; however, it was still almost identical to the 45 deg angled ribbed cases because the angled rib-induced secondary flow was strong.

2. For the cases with the transverse ribs and bleed flow, the Sherwood number ratios on the bleeding surfaces increased with the bleed ratios, but were decreased as the flow direction proceeded. Due to the rotation-induced secondary flow, high values were observed near both the walls while low values were observed in the middle region of the leading surface.
3. For the cases of the 45 deg angled ribs and bleed flow, the heat/mass transfer on the bleeding surface decreased due to the strong rib-induced secondary flow although the bleed ratios increased in contrast with the 90 deg angled ribbed cases. Further, due to the rotation-induced secondary flow, local heat/mass transfer distributions did not appear although the discrepancy between both the surfaces was shown by the deflection of the core flow.
4. The friction factor ratios increased with the rotation number only in cases with the transverse ribs and nonbleeding surfaces due to high turbulence intensity by the Coriolis force. The friction factor ratios decreased in the other cases as the flow rates and flow deflection by the Coriolis force decreased. However, the thermal performance was almost identical for all the rotation number.
5. At the maximum rotation number and bleed ratio under the tested conditions, the 90 deg rib turbulators have a cooling advantage in terms of higher heat transfer; however, the 45 deg rib turbulators have a high performance at the same coolant flow rate. Therefore, the design of the internal cooling passage should be considered with the thermal load, the operating conditions, etc.

Acknowledgment

This work was supported partially by the Korea Energy Management Corporation, through the Energy Technology Development Program.

Nomenclature

- BR = ratio of bleed flow rate to main flow rate
- d = bleed hole diameter
- D_h = hydraulic diameter
- D_{naph} = mass diffusion coefficient of naphthalene vapor in air ($\text{m}^2\ \text{s}^{-1}$)
- e = rib height
- f = friction factor, Eq. (4)
- f_0 = friction factor of a fully developed turbulent flow in a stationary smooth pipe
- h = heat transfer coefficient ($\text{W m}^{-2}\ \text{K}^{-1}$)
- h_m = mass transfer coefficient (m s^{-1})
- H = passage height
- k = thermal conductivity of coolant ($\text{W m}^{-1}\ \text{K}^{-1}$)
- $\dot{m}$ = local naphthalene mass transfer rate per unit area ($\text{kg m}^{-2}\ \text{s}^{-1}$)
- Nu = Nusselt number, hD_h/k
- p = rib-to-rib pitch
- p_h = hole to hole pitch
- Pr = Prandtl number, $\mu C_p/k$
- R = maximum radius of rotating arm
- Re = Reynolds number, $D_h u_b/\nu$
- Ro = rotation number, $D_h\Omega/u_b$
- Sc = Schmidt number, ν/D_{naph}
- Sh = Sherwood number, $h_m D_h/D_{\text{naph}}$

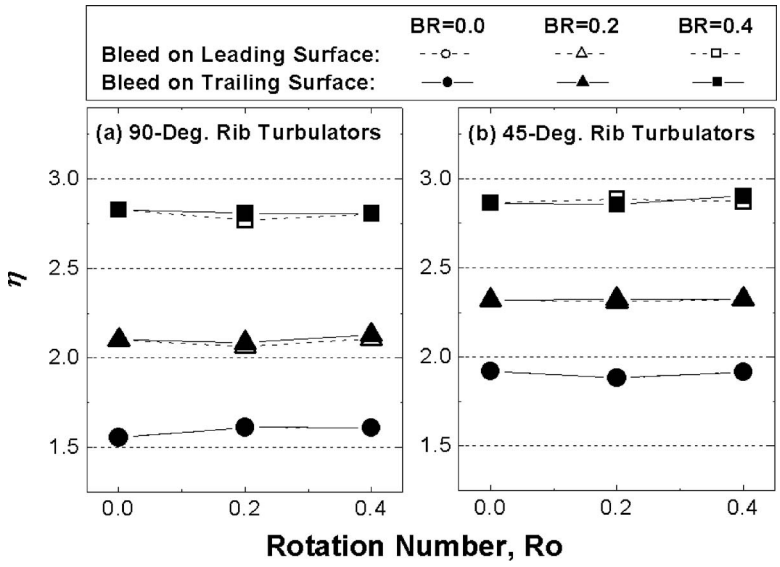

Fig. 12 Thermal performance for all tests

Sh_0 = Sherwood number of a fully developed turbulent flow in a stationary smooth pipe, Eq. (3)

$\overline{\mathrm{Sh}_0}$ = pitch averaged Sherwood number, $\int_{x_1}^{x_2}\int_{-W/2}^{W/2}\mathrm{Sh}\, dydx / \int_{x_1}^{x_2}\int_{-W/2}^{W/2} dydx$

$\overline{\mathrm{Sh}_R}$ = Sherwood number averaged over several pitches

$\bar{\overline{\mathrm{Sh}}}_R$ = mean $\overline{\mathrm{Sh}}_R$ of both the leading and trailing surfaces

u_b = passage averaged bulk velocity (m s^{-1})

W = passage width

x = coordinate and distance in the streamwise direction

y = coordinate and distance in the lateral direction

z = coordinate and distance in the vertical direction

α = attack angle of rib turbulator

Δt = runtime

Δz = sublimation depth of naphthalene surface

μ = dynamic viscosity (kg m^{-1} s^{-1})

ν = kinematic viscosity (m^2 s^{-1})

η = thermal performance, Eq. (5)

ρ_s = density of solid naphthalene (kg m^{-3})

$\rho_{v,b}$ = bulk vapor density of naphthalene (kg m^{-3})

$\rho_{v,w}$ = vapor density of naphthalene on the surface (kg m^{-3})

Ω = angular velocity (rad s^{-1})

References

[1] Han, J. C., Glicksman, L. R., and Rohsenow, W. M., 1978, "An Investigation of Heat Transfer and Friction for Rib-Roughened Surfaces," Int. J. Heat Mass Transfer, **21**, pp. 1143–1156.

[2] Kukreja, R. T., Lau, S. C., and McMillin, R. D., 1993, "Local Heat/Mass Transfer Distribution in a Square Channel With Full and V-Shaped Ribs," Int. J. Heat Mass Transfer, **36**, pp. 2013–2020.

[3] Agliga, D. A., 1994, "Convective Heat Transfer Distributions Over Plates With Square Ribs From Infrared Thermography Measurements," Int. J. Heat Mass Transfer, **36**(3), pp. 363–374.

[4] Acharya, S., Myrum, T., Qiu, X., and Sinha, S., 1997, "Developing and Periodically Developed Flow, Temperature and Heat Transfer in a Ribbed Duct," Int. J. Heat Mass Transfer, **40**, pp. 461–479.

[5] Astarita, T., Cardon, G., and Carlomagno, G. M., 1998, "Average Heat Transfer Measurements Near a Sharp 180 Degree Turn Channel for Different Aspect Ratios," *IMechE Conference Trans.: In Optical Methods and Data Processing in Heat and Fluid Flow*, London, pp. 137–146.

[6] Metzger, D. E., and Vedula, R. P., 1987, "Heat Transfer in Triangular Channels With Angled Roughness Ribs on Two Walls," Exp. Heat Transfer, **1**(1), pp. 31–44.

[7] Yang, W.-J., Zhang, N., and Chiou, J., 1992, "Local Heat Transfer in a Rotating Serpentine Flow Passage," ASME J. Heat Transfer, **114**, pp. 354–361.

[8] Iacovides, H., Jackson, D. C., Kelemenis, G., Launder, B. E., and Yuan, Y. M., 1999, "Experiments on Local Heat Transfer in a Rotating Square-Ended U-bend," Int. J. Heat Fluid Flow, **20**, pp. 302–310.

[9] Dutta, S., and Han, J. C., 1996, "Local Heat Transfer in Rotating Smooth and Ribbed Two-Pass Square Channels With Three Channel Orientations," ASME J. Heat Transfer, **118**, pp. 578–576.

[10] Murata, A., and Mochizuki, S., 1999, "Effect of Cross-sectional Aspect Ratio on Turbulent Heat Transfer in an Orthogonally Rotating Rectangular Smooth Duct," Int. J. Heat Mass Transfer, **42**, pp. 3803–3814.

[11] Taslim, M. E., Li, T., and Spring, S. D., 1995, "Experimental Study of the Effects of Bleed Holes on Heat Transfer and Pressure Drop in Trapezoidal Passages With Tapered Turbulators," ASME J. Turbomach., **117**, pp. 281–289.

[12] Shen, J. R., Wang, Z., Ireland, P. T., Jones, T. V., and Byerley, A. R., 1996, "Heat Transfer Enhancement Within a Turbine Blade Cooling Passage Using Ribs and Combinations of Ribs With Film Cooling Holes," ASME J. Turbomach., **118**, pp. 428–434.

[13] Thurman, D., and Poinastte, P., 2001, "Experimental Heat Transfer and Bulk Air Temperature Measurements for a Multipass Internal Cooling Model With Ribs and Bleed," ASME J. Turbomach., **123**, pp. 90–96.

[14] Ekkad, S. V., Huang, Y., and Han, J. C., 1998, "Detailed Heat Transfer Distributions in Two-Pass Square Channels With Rib Turbulators and Bleed Holes," Int. J. Heat Mass Transfer, **41**, pp. 3781–3791.

[15] Kim, K. M., Kim, S. I., Jeon, Y. H., Lee, D. H., and Cho, H. H., 2007, "Detailed Heat/Mass Transfer Distributions in a Rotating Smooth Channel With Bleed Flow," ASME J. Heat Transfer, **129**(11), pp. 1538–1545.

[16] Jeon, Y. H., Park, S. H., Kim, K. M., Lee, D. H., and Cho, H. H., 2007, "Effects of Bleed Flow on Heat/Mass Transfer in a Rotating Rib-Roughened Channel," ASME J. Turbomach., **129**(3), pp. 636–642.

[17] Ambrose, D., Lawrenson, I. J., and Sparke, C. H. S., 1975, "The Vapor Pressure of Naphthalene," J. Chem. Thermodyn., **7**, pp. 1173–1176.

[18] Goldstein, R. J., and Cho, H. H., 1995, "A Review of Mass Transfer Measurements Using Naphthalene Sublimation," Exp. Therm. Fluid Sci., **10**, pp. 416–434.

[19] Kline, S. J., and McClintock, F. A., 1953, "Describing Uncertainty in Single-Sample Experiments," Mech. Eng. (Am. Soc. Mech. Eng.), **75**, pp. 3–8.

[20] McAdams, W. H., 1942, *Heat Transmission*, 2nd ed., McGraw-Hill, New York.

[21] Petukhov, B. S., 1970, *Advances in Heat Transfer*, Vol. 6, Academic, New York, Vol. 6, pp. 503–504.

[22] Ekkad, S. V., and Han, J. C., 1997, "Detailed Heat Transfer Distributions in Two-Pass Square Channels With Rib Turbulators," Int. J. Heat Mass Transfer, **40**, pp. 2525–2537.